energies

MDPI

Article

Depositional Environment and Organic Matter Enrichment of Early Cambrian Niutitang Black Shales in the Upper Yangtze Region, China

Peng Xia [1,2,3,*], Fang Hao [3], Jinqiang Tian [3], Wenxi Zhou [1], Yong Fu [1,2], Chuan Guo [1,2], Zhen Yang [1], Kunjie Li [4] and Ke Wang [1,2]

[1] Resource and Environmental Engineering College, Guizhou University, Guiyang 550025, China; gzzhouwenxi@126.com (W.Z.); byez1225@126.com (Y.F.); cguo@gzu.edu.cn (C.G.); cugbyzh@163.com (Z.Y.); kwang5@gzu.edu.cn (K.W.)
[2] Key Laboratory of Ministry of Education for Geological Resources and Environment, Guiyang 550025, China
[3] School of Geosciences, China University of Petroleum, Qingdao 266580, China; haofang@cup.edu.cn (F.H.); tianjingqiang@cup.edu.cn (J.T.)
[4] Huaxin Gas Group Company Limited, Taiyuan 030026, China; marden2008@163.com
* Correspondence: pxia@gzu.edu.cn

Abstract: Natural gas generation is the result of organic matter degradation under the effects of biodegradation and thermal degradation. Early Cambrian black shales in the Upper Yangtze Region are rich in organic matter and have shown great shale gas potentiality in recent years. Nevertheless, the enrichment mechanism and distribution of organic matter in these black shales between different sedimentary settings, such as intra-platform basin, slope, and deep basin, are still poorly understood. In this paper, based mainly on elemental geochemistry, a comprehensive study of the marine redox conditions, primary productivity, sedimentation rate, terrigenous input, hydrothermal activity, and water mass restrictions was conducted on the Early Cambrian Niutitang black shale in the Upper Yangtze Region. Our data showed that an intra-platform basin received a higher terrigenous input and that it deposited under more restricted conditions than the slope and deep basin settings. The primary productivity in the slope and deep basin settings was higher than that in the intra-platform basin setting. In the intra-platform basin, the productivity increased from its inner part to its margin. For the slope and deep basin settings, the high paleoproductivity generated large amounts of organic matter and its preservation was synergistically affected by the redox conditions. In contrast to the slope and deep basin, the preservation of organic matter in the inner part of the intra-platform basin was mainly controlled by redox conditions because the paleoproductivity in it was much lower than in the slope and deep basin settings. The intra-platform basin margin was the most favorable area for accumulating organic matter.

Keywords: Early Cambrian; paleoenvironment; black shale; shale gas; Southern China

check for updates

Citation: Xia, P.; Hao, F.; Tian, J.; Zhou, W.; Fu, Y.; Guo, C.; Yang, Z.; Li, K.; Wang, K. Depositional Environment and Organic Matter Enrichment of Early Cambrian Niutitang Black Shales in the Upper Yangtze Region, China. *Energies* **2022**, *15*, 4551. https://doi.org/10.3390/en15134551

Academic Editors: Jing Li, Yidong Cai and Lei Zhao

Received: 12 May 2022
Accepted: 15 June 2022
Published: 22 June 2022

Publisher's Note: MDPI stays neutral with regard to jurisdictional claims in published maps and institutional affiliations.

Copyright: © 2022 by the authors. Licensee MDPI, Basel, Switzerland. This article is an open access article distributed under the terms and conditions of the Creative Commons Attribution (CC BY) license (https://creativecommons.org/licenses/by/4.0/).

1. Introduction

The development of black shales mostly occurs during particular periods of geological history, and they not only record the changes in the paleoenvironment, paleoclimate, and paleontology, but also contain large quantities of metal-rich minerals and oil and gas resources [1–4]. The Early Cambrian Niutitang black shale in the Guizhou Province and northwest Hubei Province is an iconic deposit dating from the Neoproterozoic to the Early Paleozoic Era in Southern China [5,6]. This black shale, which is rich in shale gas resources, contains 3.55×10^{12} m^3 shale gas in the Upper Yangtze Region alone [7]. Shale gas production in China reached 228×10^8 m^3 per annum in 2021, but this shale gas was mainly extracted from the Late Ordovician Wufeng and Early Silurian Longmaxi formations in the Sichuan Basin [4,8]. In contrast, the development of shale gas from the

Early Cambrian Niutitang black shale has been very limited, even though abundant gas is preserved in it.

The abundance, type, and maturity of organic matter are three key parameters determing gas potentiality in shales [9,10]. Organic matter accumulation is the first requirement for generating and preserving shale gas, and accurately identifying the organic matter accumulation mechanism is helpful for shale gas development. Previous studies have focused on the depositional environment, lithofacies, mineral composition and genesis, and pore structure of the Early Cambrian Niutitang black shale. These studies concluded that this black shale is rich in organic matter, dominated by quartz and clay minerals, and strongly heterogeneous [7,11–18]. However, the mechanism of organic matter accumulation in this black shale has been debated for many years because it is a very complicated biogeochemical process [19–21].

Currently, it is widely acknowledged that organic matter accumulation and preservation in sedimentary strata are determined by a combination of primary productivity, paleoredox conditions, and sedimentation rate in sedimentary basins [21–24]. Primary productivity determines the input quantity of the organic matter, while the preservation of this organic matter is controlled by the paleoredox conditions and sedimentation rate [22,25]. A high sedimentation rate not only promotes organic matter preservation by reducing its exposure time under oxic conditions, but also dilutes the organic matter [23]. Moreover, other factors such as hydrothermal activity, upwelling, river input, continental weathering, and water mass restrictions also influence organic matter accumulation [6,21,26]. Owing to the combination of the abovementioned influences, it is difficult to accurately explain the organic matter accumulation mechanisms of black shale.

Taking the Early Cambrian Niutitang black shale as an example, some researchers have reported that an anoxic paleoenvironment is the most significant factor affecting organic matter accumulation [27,28], while other researchers argue that a high productivity is the most important factor [14,29]. Still, others have concluded that the organic matter preserved in this black shale was accumulated by a combination of ideal preservation conditions and a high productivity [30,31]. It is worth noting that during the deposition of the Early Cambrian Niutitang black shale, the Upper Yangtze Region mainly included the intra-platform basin, slope, and deep basin settings [32], and the redox conditions, hydrothermal activity, and amount of terrigenous flux in these settings were different [6,26,33,34]. Moreover, Zhu et al. (2019) [7] reported that the total organic carbon (TOC) content of the Early Cambrian Niutitang black shale decreases from the intra-platform basin margin, through the slope and inner intra-platform basin, to the deep basin and shore settings in the Upper Yangtze Region (Figure 1). Thus, the organic matter accumulation mechanism may be completely different for the various settings. Previous studies have discussed the distribution of the organic matter content in the Early Cambrian Niutitang black shale [14,26,35–37], while the differences in organic matter accumulation and its mechanism among the contemporaneous sediments of the different sedimentary settings (such as intra-platform basin, slope, and deep basin) are still unclear.

The primary goals of this study were to determine the characteristics of the paleoredox conditions, paleoproductivity, paleoclimate, hydrothermal activity, terrigenous flux, and water mass restrictions of the different settings (intra-platform basin, through slope, to deep basin) and to compare the organic matter accumulation mechanisms among these settings during the sedimentation of the Early Cambrian Niutitang black shale. Geochemical proxies such as U/Th, V/(V + Ni), V/Cr, Ni/Co, biogenic Ba (Ba_{bio}) and Si (Si_{bio}), and δCe were used to reconstruct the paleoenvironment. Then, organic geochemical methods were combined with these geochemical proxies to investigate the organic matter accumulation mechanism. The results of this study improve our understanding of the distribution of the organic matter in the Early Cambrian Niutitang black shale and provide important information for predicting favorable areas for shale gas production.

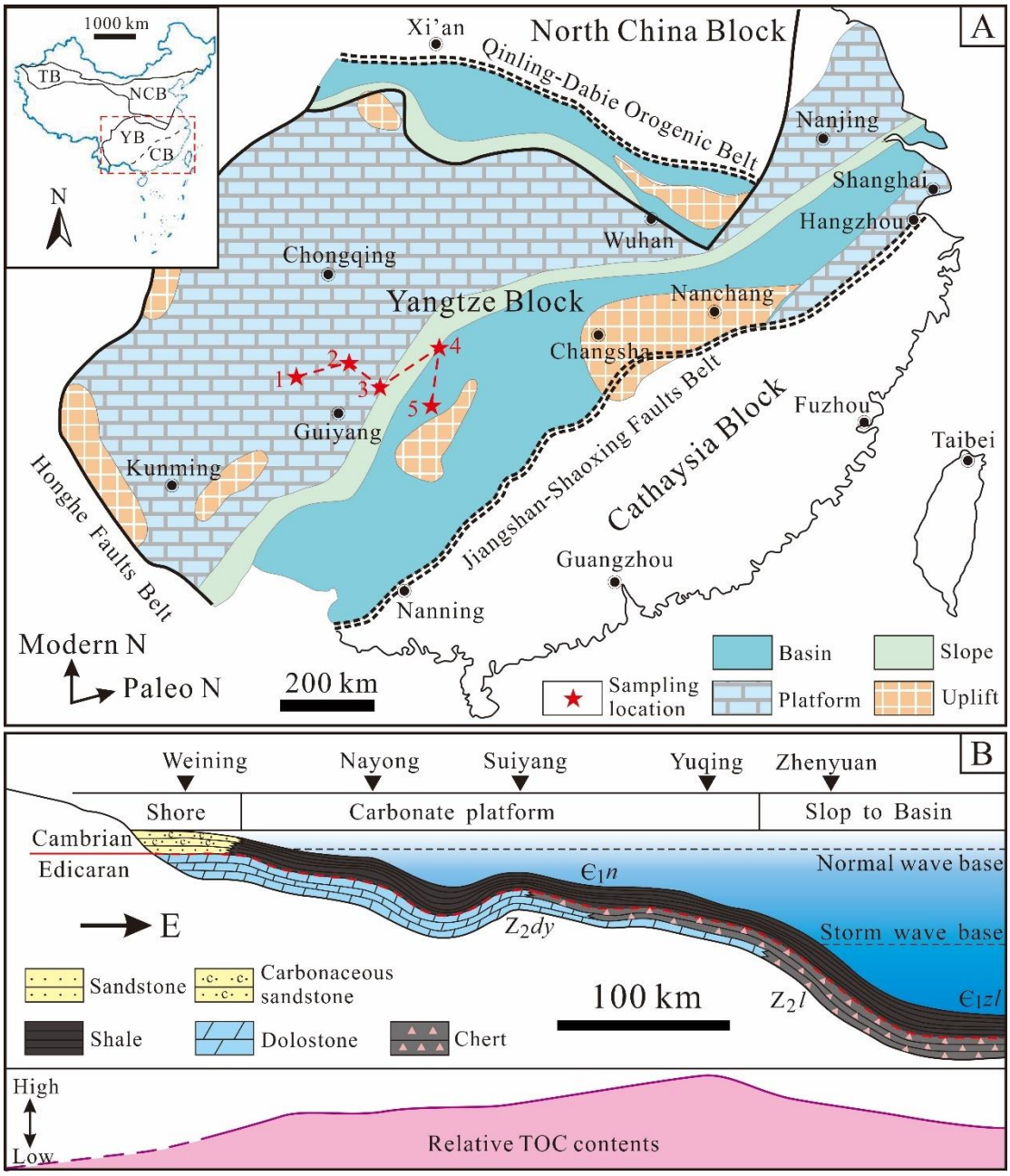


Figure 1. (**A**) Paleoenvironment reconstruction of the Yangtze Block during the Ediacaran–Cambrian transition stage illustrating the geological setting of the study area (modified from [32,38]). The red stars are the sample locations. 1—Yankong section, 2—Songlin section, 3—Yonghe section, 4—well ZK102, and 5—well ZK205. (**B**) Sketch showing the sedimentary environment and the relative TOC contents of the Lower Cambrian black shale, Guizhou Province (modified from [39], and the TOC data are from [7]). Z_2dy—the Ediacaran Dengying Formation, Z_2l—the Ediacaran Laobao Formation, $\in_1 n$—the Cambrian Niutitang Formation, and $\in_1 zl$—the Cambrian Zhalagou Formation.

2. Geological Setting

The South China Continent and the Jiangnan orogeny gradually developed around 880–860 Ma as a result of the collision between the Yangtze Block and Cathaysia Block [40,41]. This coupled South China Continent was then subjected to intense rifting during 850–820 Ma, resulting in its gradual separation into the Yangtze Block and Cathaysia Block once again; the Nanhua Basin was developed between these two blocks [41,42]. In the Ediacaran, especially during the Ediacaran–Cambrian transition stage, the Yangtze Block was subjected

to intense extension and block tilting, resulting in the development of a carbonate platform on the paleohigh surrounded by a large-scale open siliceous basin (Figure 1A) [14,32,43].

The Yangtze Block developed sedimentary setting belts, generally including an intra-platform basin, slope, and deep basin, from northwest to southeast during the Ediacaran–Cambrian transition stage [32]. Interestingly, the Early Cambrian black shale has completely different stratigraphic contact relationships in the intra-platform basin compared to the slope and deep basin [6,18]. In the intra-platform basin setting, the Early Cambrian black shale of the Niutitang Formation unconformably overlies the dolostone of the Ediacaran Dengying Formation (Figures 1B and 2). However, this black shale conformably overlies the chert of the Ediacaran Laobao Formation (Figures 1B and 2)–a contemporaneous sediment of the Dengying dolostone–in the slope and deep basin settings [18,44,45]. Thus, this black shale is considered to be the key layer representing the transition from the Ediacaran to the Cambrian in the Yangtze Block and the change in the environment and climate [6,11,26,46], and it is one of the most significant shale gas reservoirs in China [4,7].

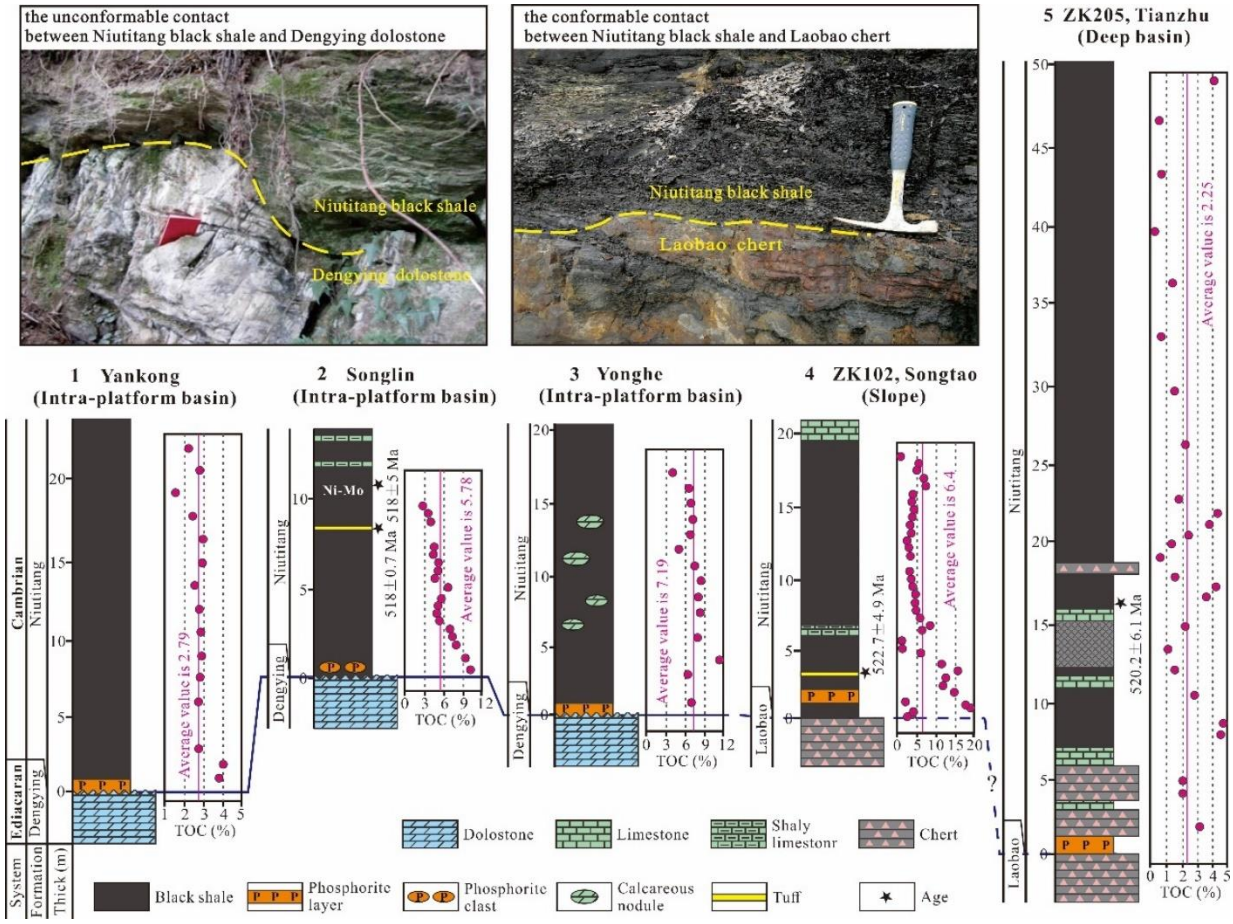


Figure 2. Contact relationship between the Ediacaran and Cambrian strata, and the stratigraphic columns and TOC contents of the Early Cambrian black shale. The ages are cited from [47–49].

3. Materials and Methods

3.1. Sample Collection and Preparation

A total of 110 fresh black shale samples were collected from three sections and two wells for the geochemical analyses conducted in this study (Figure 1A), and all the samples were sealed in plastic bags to ensure as little contamination as possible. Among them, 15 samples were from the Yankong section in northwestern Guizhou Province; 18 samples were from the Songlin section in northern Guizhou Province; 14 samples were from the Yonghe section in southern Guizhou Province; and 37 and 26 samples were from well ZK102 in northeastern Guizhou Province and well ZK205 in southeastern Guizhou

Province, respectively. All the potentially weathered surfaces, visible pyrite grains, and post-depositional veins were removed from each sample. Then, the samples were cut into small pieces. Approximately 100 g of the freshest pieces was crushed to powder (<200 mesh) using a tungsten carbide crusher.

3.2. Analytical Methods

The TOC content and element concentrations (including major, trace, and rare earth elements) of all sample powders were measured after they were acidified using 5% HCl to remove the carbonates, and neutralized to a pH of 7.0 by adding deionized water. The measurement of TOC content was conducted at the Central Laboratory of Geological Sciences, China National Petroleum Corporation (CNPC) Petroleum Exploration and Development Institute, using a LECO CS-230 sulfur-carbon analyzer.

The analysis of the element concentrations was conducted at the Institute of High Energy Physics, Chinese Academy of Science, following four Chinese National Standards (GBW07103, GBW07104, GBW07107, and GBW07108). Prior to the major element analysis, about 200 g of sample powder was dried at 100 °C to remove any moisture. A $Li_2B_4O_7$-$LiBO_2$-LiF mixture (about 6 g), ammonium nitrate (0.4 g), and 1 mg of sample powder were accurately weighted into a crucible, and the crucible was then slightly shaken to ensure that the solid particles within it were completely mixed. About 0.25 mL of lithium bromide solution was added to the mixture. Subsequently, the mixture in the crucible was fused at 1080 °C for 10 min to generate a glass bead, and the generated glass bead was measured with an X-ray fluorescence spectrometer.

For the trace and rare earth element content analyses, about 300 mg of sample powder was ashed at 850 °C for 8 h to remove any volatiles before the analysis. A mixture of HF, HNO_3, and HCl was used to dissolve each ashed sample (about 50 mg). After this digestion, the solution was diluted using 2% nitric acid and then measured using an inductively coupled plasma mass spectrometer. The procedures for the element analyses have also been described by Li et al. (2010, 2020) [11,12]. The results of the trace and rare earth element analyses have also been presented in our previous publications [15,18].

4. Results

4.1. Total Organic Carbon Content

The TOC contents of the shale samples are shown in Figure 2, and they vary from 0.29% to 28% with an average of 4.93%. Among the sampling profiles, the TOC contents decrease from the Yonghe section, through the Songlin section and well ZK102, to the Yankong section and well ZK205. In the Yonghe section, the average TOC content is as high as 7.19%. In the Songlin section and well ZK102, the TOC contents are 2.93–10.2% (5.78% on average) and 1.19–28% (6.4% on average), respectively. In the Yankong section and well ZK205, the TOC contents are as low as 1.66–4% (2.79% on average) and 0.29–4.7% (2.25% on average), respectively (Figure 2).

4.2. Major Elements

The experimental results of the major elements are presented in the Supplementary Materials. In general, SiO_2 and Al_2O_3 are the major components of the shale samples from the Yankong section (average SiO_2 and Al_2O_3 contents of 57.65% and 15.5%, respectively), Songlin section (average content of SiO_2 is 65.9% and Al_2O_3 is 12.92%), Yonghe section (average SiO_2 and Al_2O_3 contents of 72% and 8.93%, respectively), and well ZK102 (average SiO_2 and Al_2O_3 contents of 52.7% and 11.13%, respectively), while the shale samples from well ZK205 have much lower Al_2O_3 contents (0.21–8.17%, 3.75% on average).

4.3. Trace Elements

The trace element data are presented in the supplementary materials. The total trace element concentrations (40 trace elements) of the shale samples range from 1058.27 to 46,941.16 ppm. Among the sampling profiles, the Yonghe section has the highest trace

element concentrations, with an average concentration of 8557.21 ppm. In addition, the shale samples from the intra-platform basin setting (average concentrations of 3223.94 and 4809.08 ppm for the Yankong section and the Songlin section, respectively) have much lower trace element concentrations than the samples from the slope and deep basin settings (average concentrations of 7459.64 and 7982.13 ppm for wells ZK102 and ZK205, respectively).

The enrichment factor is a good indicator for elemental enrichment or depletion and the enrichment factors of trace elements were calculated using the following

$$X_{ef} = (X/Sc)_{sample}/(X/Sc)_{UCC}$$

where X is the target trace element (such as Ni, Ba, Mo, U, and V), and UCC is the average composition of the upper continental crust [50]. The calculated results show that (1) the shale samples in this study are rich in Ni, Mo, Re, U, V, Cr, Cu, Zn, Ga, Cd, In, Sb, and Ba in contrast to the upper continental crust (Figure 3); and (2) the shale samples indicating the intra-platform basin setting have higher enrichment factors than the shale samples correlated to the slope and deep basin settings (Figure 3).

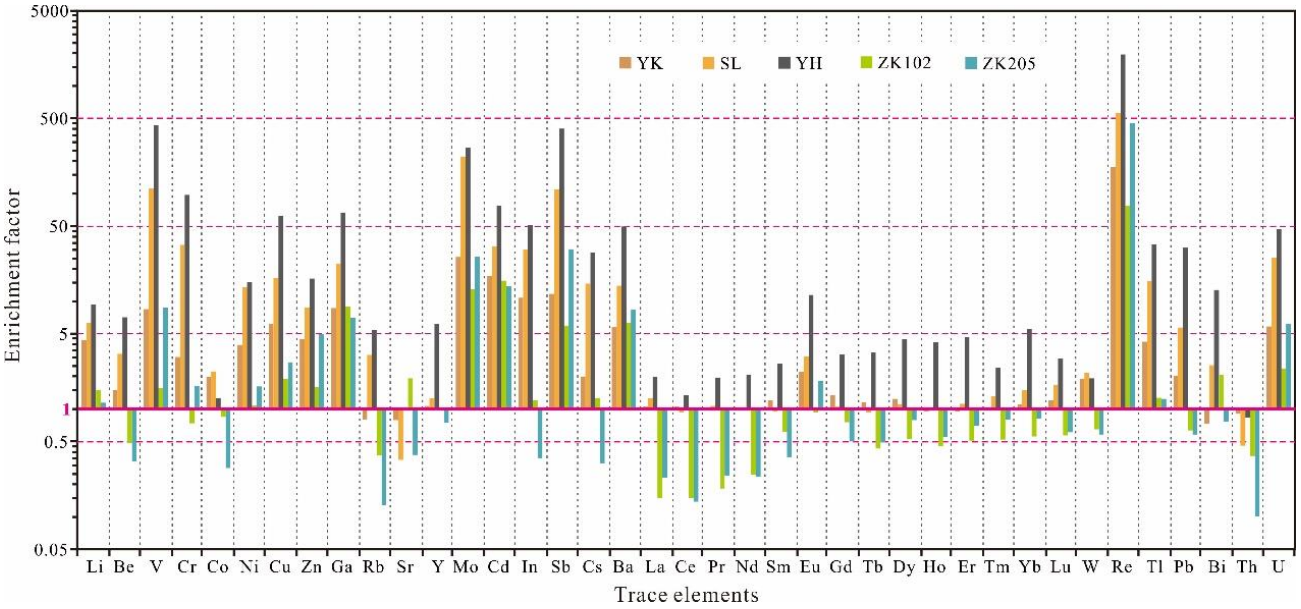


Figure 3. The average enrichment factors of trace elements in the Early Cambrian black shale.

4.4. Rare Earth Elements (REEs)

The rare earth element (REE) concentrations are presented in the supplementary materials and the REEs pattern of NASC was used to normalize the REEs data in this study [51]. Figure 4 shows the REE distribution patterns, total REE (∑REE) contents, and the ratios of light REEs and heavy REEs (LREE/HREE) of the shale samples in this study. The ∑REE values of the shale samples vary from 2.46 to 230.02 ppm (47.17 ppm on average), and the LREE/HREE ratios are 1.87–48.87, with an average of 12.15, indicating light REE enrichment. The Yankong section has the highest average ∑REE value of 85.48 ppm. The average ∑REE values of samples from wells ZK102 and ZK205 (50.37 and 43.47 ppm, respectively) are much lower than in the Yankong section, but they are significantly higher than in the Songlin and Yonghe sections (28.68 and 28.31 ppm, respectively). The LREE/HREE ratios decrease from the intra-platform basin to the slope and deep basin. The Yankong and Songlin sections of the intra-platform basin setting have ratios of 25.07 and 23.47, respectively. In contrast, the ratios of wells ZK102 (slope setting) and ZK205 (deep basin setting) are as low as 7.07 and 5.71, respectively. The Yonghe section is located in the transition zone between the intra-platform basin and slope (Figures 1 and 2), and it has a medium ratio (9.15) among the sampling profiles studied (Figure 4).

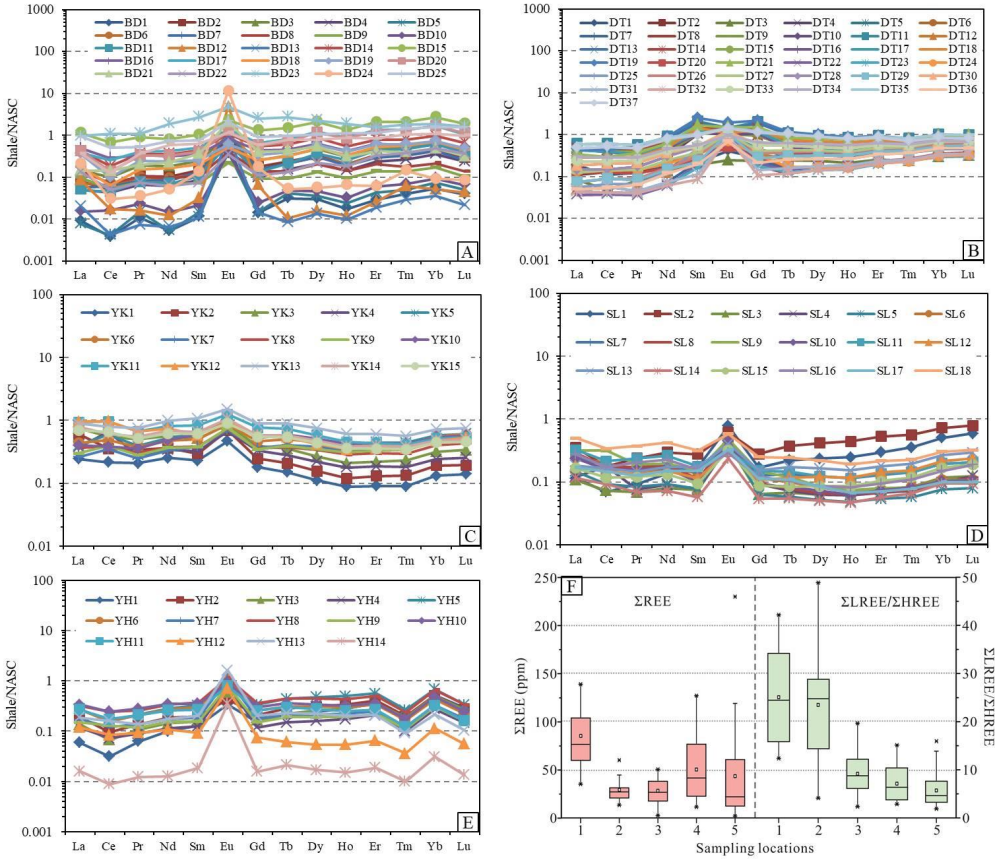


Figure 4. Rare earth element (REE) distribution patterns for the Early Cambrian black shale, and REE contents and light REE to heavy REE (LREE/HREE) ratios. (**A**) ZK205 well, (**B**) ZK102 well, (**C**) Yankong section, (**D**) Songlin section, (**E**) Yonghe section, (**F**) REE contents and light REE to heavy REE (LREE/HREE) ratios (1—Yankong section, 2—Songlin section, 3—Yonghe section, 4—well ZK102, and 5—well ZK205. Box-plot: asterisks are the maximum and minimum values, hollow square is average value).

5. Discussion

5.1. Hydrothermal Influences

Hydrothermal fluids carry many ore-forming elements (such as Mn, Ba, Cu, Pb, Fe, and Zn), and these elements can be transported and precipitated in response to changes in the physical and chemical conditions [52,53]. As a result, the contents of these elements in the sediments will be abnormally and radially distributed around the center of the hydrothermal fluid input channel. Thus, anomalous abundances of these elements are one of the most important geochemical characteristics of hydrothermal sediments and can be used to distinguish between hydrothermal sediments and normal sediments [26,54–56]. In contrast to normal sediments, hydrothermal sediments are generally enriched in elements such as Si, Mn, P, Pb, Zn, Cu, Ba, Fe, Sr, and U, while they are depleted in elements such as Al, Ti, Mg, Cr, Th, Zr, and Rb. As shown in Figure 5, the contents of the major element set Si+Fe+Mn+P and trace element set Cu+Pb+Zn+Ba+Sr+U in the shale samples are generally higher than those in the crust, while the contents of the major element set Al+Ti+Mg and trace element set Cr+Th+Rb are lower than those in the crust, indicating that the sedimentation of this shale was related to a hydrothermal event. In particular, in the slope and deep basin regions, the thick chert beds at the top of the Ediacaran strata (Figures 1B and 2) indicate that the hydrothermal activities mainly occurred in these regions during the Ediacaran–Cambrian transition stage. Wei et al. (2018) [57] suggested that the mounded cherts in the Yangtze Block were deposited in a syngenetic fault zone on the margin of the basin, and they are the results of strong submarine hydrothermal activities.

In this study, bedded cherts were observed in the slope (Laobao Formation, well ZK102) and deep basin (Laobao Formation and the bottom of the Niutitang Formation, well ZK205) regions, but no mounded chert was observed in these regions, indicating that hydrothermal activities occurred in the slope and deep basin regions during the Ediacaran–Cambrian transition stage, and the wells (ZK102 and ZK205) are not located in the central area of the hydrothermal activities.

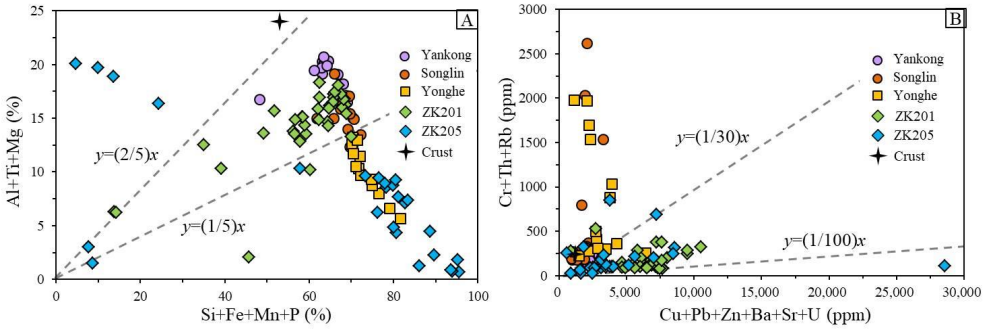


Figure 5. Relationships between different (**A**) major element sets and (**B**) trace element sets for the Early Cambrian black shale.

Sediments affected by hydrothermal activities are characterized by (1) relatively low REE abundances, (2) pronounced enrichment of HREEs relative to LREEs, and (3) positive Eu anomalies [51,53,58]. The REE distribution patterns and the ranges of the REE abundances and LREE/HREE ratios of the shale samples are shown in Figure 4. The samples from the two wells (wells ZK102 and ZK205) and the Yonghe section have relatively low REE abundances and ∑LREE/∑HREE ratios, and large positive Eu anomalies, confirming the effects of hydrothermal activities on the Early Cambrian Niutitang black shale from the intra-platform basin margin, through the slope, to the deep basin. It should be noted that the samples from the Songlin section (intra-platform basin setting; Figures 1 and 2) also have relatively low REE abundances and positive Eu anomalies. However, these samples have high proportions of LREEs and Cr+Th+Rb concentrations (Figure 5B), suggesting that their positive Eu anomalies and low REE abundances did not originate from hydrothermal activities. The samples from the intra-platform basin setting may have been significantly affected by the terrigenous flux.

5.2. Paleoclimate and Terrigenous Flux

In general, a warm and humid tropical climate triggers stronger chemical weathering than a cold and dry climate. The chemical index of alteration (CIA) is one of the most effective proxies evaluating the intensity of chemical weathering, which is expressed as follows:

$$\mathrm{CIA} = \mathrm{molar}[\mathrm{Al_2O_3}/(\mathrm{Al_2O_3} + \mathrm{CaO*} + \mathrm{Na_2O} + \mathrm{K_2O})] \times 100,$$

where CaO* represents the CaO in the silicate minerals only [59,60], which has been corrected using the P_2O_5 data (CaO* = mole (CaO-P_2O_5) × 10/3). If the remaining molar amount of CaO is less than that of Na_2O, CaO* should be used as the CaO value; otherwise, the CaO* should be equivalent to the Na_2O value [61]. It should be noted that K-metasomatism of shales has a large effect on the CIA value; thus, it is necessary to make corrections using the Al_2O_3 − (CaO* + Na_2O) − K_2O (A-CN-K) ternary diagram [62].

The shale samples from the intra-platform basin (including the Yankong, Songlin, and Yonghe sections; Figures 1 and 2) generally exhibit moderate–high CIA values (Yankong section: 73.1 ± 2.7; Songlin section: 75.0 ± 2.7; and Yonghe section: 78.7 ± 7.0; Figure 6), suggesting that their source rocks underwent intense weathering under a warm and humid climate condition. In contrast, the slope (ZK102 well) to deep basin (ZK205 well) setting samples have low–moderate CIA values of 69.2 ± 7.1 in well ZK102 and 69.7 ± 8.4 in

well ZK205 (Figure 6). These values are indicative of weak chemical weathering in the source area, likely under a cooler and drier condition [6,12]. This spatiotemporal chemical weathering intensity pattern implies that the influx of terrigenous sediments to the intra-platform basin may have been different from that to the slope and deep basin settings. Combining results from this study and previous research, we suggest that the influx to the intra-platform basin was mainly from the Yangtze Block, while that to the slope and deep basin region was partly from the Cathaysia Block [12,16,63].

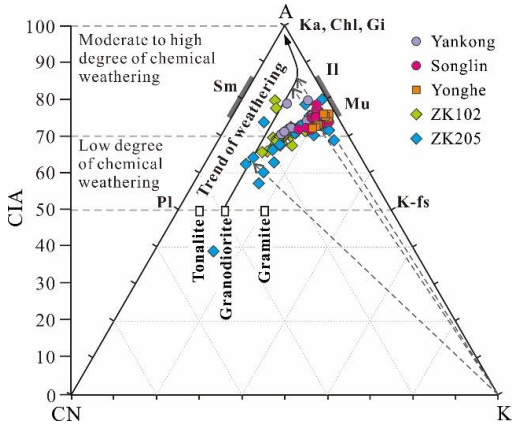


Figure 6. A-CN-K ternary diagram showing the diagenetic K-metasomatism of the Early Cambrian black shales. The associated range of the CIA values is also indicated. A—Al_2O_3; CN—CaO* + Na_2O; K—K_2O; CIA—chemical index of alteration; Ka - kaolinite; Chl—chlorite; Gi—gibbsite; Sm—smectite; Il—illite; Mu—muscovite; Pl—plagioclase; and K-fs—K-feldspar.

Elements such as Al, Ti, Th, and Zr are mainly from continental rocks and are not significantly affected by diagenesis and weathering; thus, they are considered to be indicators of the terrigenous flux [64]. Aluminum (Al) generally exists as aluminosilicate clay minerals, while Ti, Th, and Zr are usually contained in clays and heavy minerals [65]. Therefore, the Ti/Al, Th/Al, and Zr/Al ratios can indicate the input of coarse terrigenous clasts. In this study, Al, Ti, and Th were used as indicators of the terrigenous flux of the Early Cambrian Niutitang black shale, and the results are shown in Figure 7. The Yankong, Songlin, and Yonghe sections, along with well ZK102, exhibit high Al and Ti concentrations, especially in the Yankong (average concentrations of Al = 15.50%; Ti = 0.71%) and Songlin (Al = 12.92%; Ti = 0.68%) sections, which are much higher than those of the samples from well ZK205 (Al = 3.75%; Ti = 0.25%). The changes in these contents indicate that the terrigenous input to the deep basin was much lower than that to the intra-platform basin. It should be noted that Al, Ti, and Th have significant negative correlations with the TOC content for the intra-platform basin (Figure 7), suggesting that the terrigenous input had a dilution effect on the organic matter enrichment of the shale.

5.3. Sedimentation Rate

Rare earth elements (REEs) are transported into the ocean with suspended particles and detrital minerals, and the residence time of these particles and minerals in the sea water determines the degree of differentiation of the REEs [66]. Generally, a fast sedimentation rate corresponds to a moderate La_N/Yb_N ratio and a low Nd concentration, while a slow sedimentation rate results in differentiation between La and Yb and the enrichment of Nd [66–69]. As shown in Figure 8, wells ZK102 and ZK205 have lower La_N/Yb_N ratios and approximately equal Nd concentrations compared to the Yankong and Songlin sections, indicating that the sedimentation rate in the slope and deep basin settings was slightly faster than that in the intra-platform basin during the Ediacaran–Cambrian transition stage. This result conflicts with the general belief that the intra-platform basin has a faster sedimentation rate than the slope and deep basin settings. Thus, we speculate that the

higher Yb concentration in shale samples from wells ZK102 and ZK205 is the result of hydrothermal activities and upwelling events.

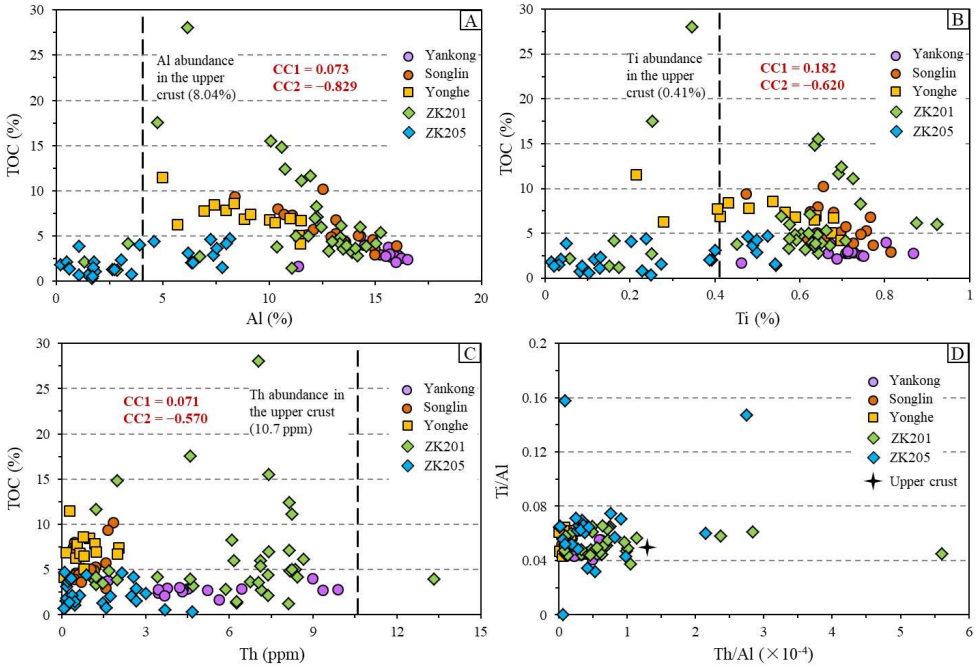


Figure 7. Plots of TOC versus (**A**) Al, (**B**) Ti, and (**C**) Th, and (**D**) plot of Ti/Al versus Th/Al. CC1—correlation coefficient of each element concentration and TOC content of all the black shales (including Yankong, Songlin, and Yonghe sections and wells ZK102 and ZK205); CC2—correlation coefficient of each element concentration and TOC content of black shales from the intra-platform basin (including Yankong, Songlin, and Yonghe sections).

5.4. Paleoproductivity

Various geochemical proxies have been effectively used to reconstruct paleoproductivity, such as the TOC content, biogenic barium (Ba_{bio}) and silica (Si_{bio}), phosphate, nutrient elements (Ni, Cu, and Zn), N and C isotopes, and biomarkers [64,70–73]. Because only a small part of the organic matter can be preserved during the stages of its passage through the water column and diagenesis, the measured TOC content of the shale is controlled by a combination of paleoproductivity, paleoredox conditions, and dilution. Some biomarkers are inaccurate when applied to over-mature shale [74]. Given the uncertainties involved in estimating the paleoproductivity based on the TOC content and biomarkers, other geochemical indicators, including Ba_{bio}, Si_{bio}, Ni+Cu+Zn, and phosphate, were used in this study (Figure 9).

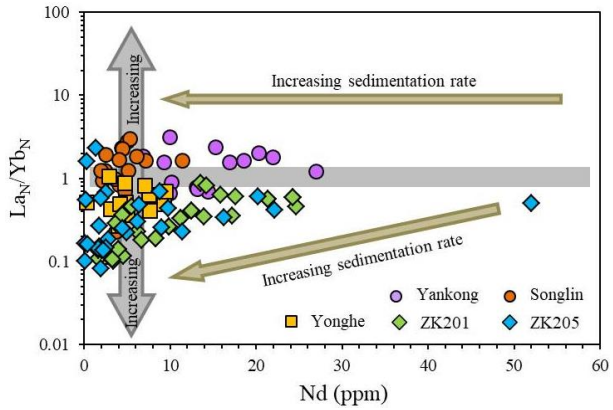


Figure 8. Plot of La_N/Yb_N versus Nd showing the sedimentation rate of the Early Cambrian black shale.

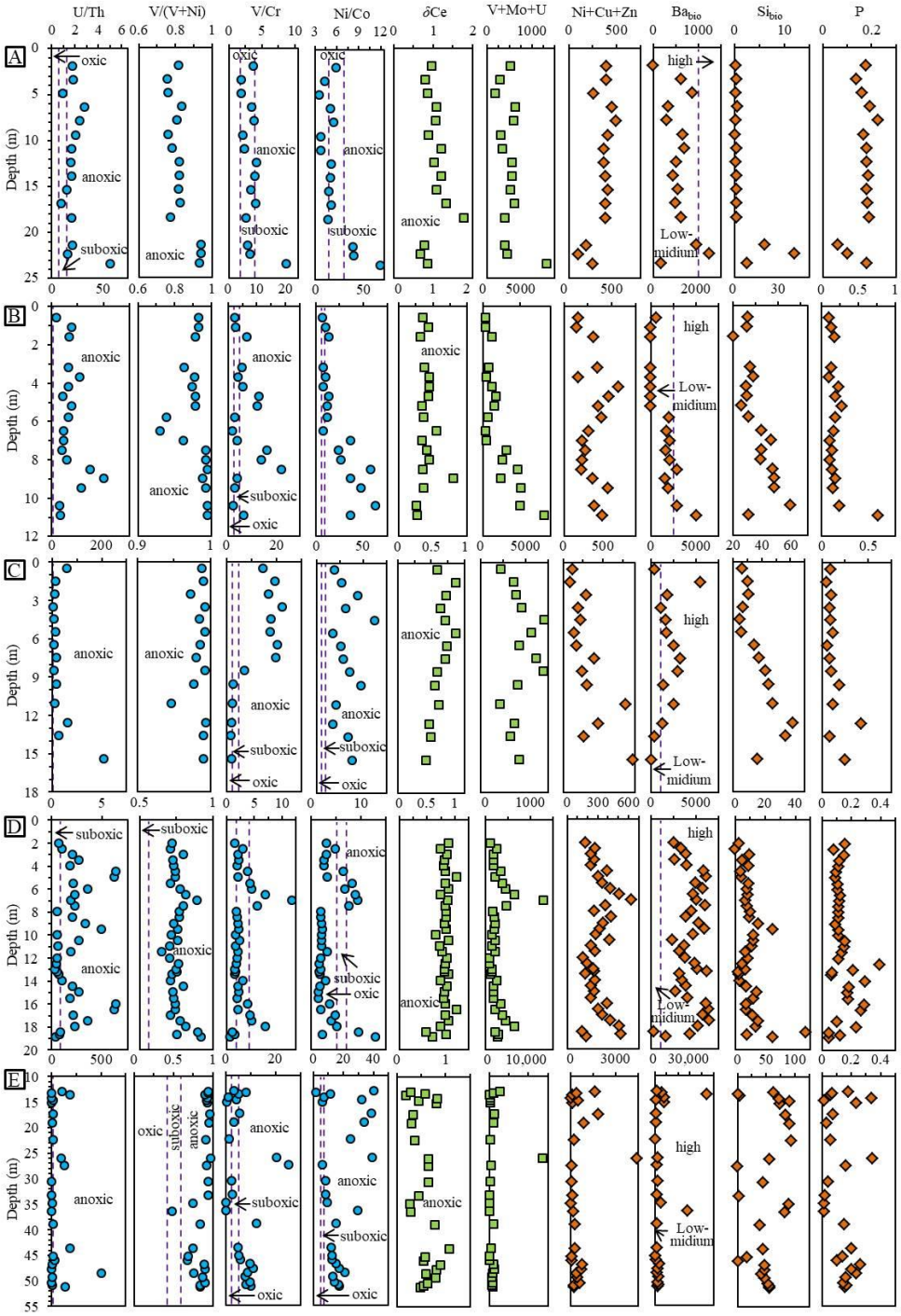


Figure 9. Stratigraphic variations in the paleoproductivity and paleoredox proxies for the (**A**) Yankong section, (**B**) Songlin section, (**C**) Yonghe section, (**D**) well ZK102, and (**E**) well ZK205. The unit for V+Mo+U, Ni+Cu+Zn, and Ba_{bio} is ppm, the unit for Si_{bio} and P is %, and U/Th, V/(V + Ni), V/Cr, Ni/Co, and δCe are dimensionless.

In a shale sample, the fraction of the Ba_{bio} is in excess relative to normal terrigenous material, and it can be calculated using the following formula [75]:

$$Ba_{bio} = Ba_{total} - \left[Al_{total} \times (Ba/Al)_{terrigenous}\right],$$

where Ba_{total} is the total amount of barium in the sample, ppm; Al_{total} is the total amount of aluminum in the sample; and $(Ba/Al)_{terrigenous}$ is the average Ba/Al ratio of the upper crust.

The Ba_{bio} value appears to originate from the decayed organic matter. This organic matter was produced by the surface productivity. In the ideal case, for shale, a high Ba_{bio} content indicates a high paleoproductivity [75]. However, barium is an unstable element under anoxic to euxinic conditions, which can be recycled into the overlying water column under the effects of sulfate reducing bacteria (such as bacterial sulfate reduction, BSR). Among the shale samples in this study, the Ba_{bio} contents of the intra-platform basin range from 11.05 to 5508.97 ppm, with an average of 1141.38 ppm, while those of the slope and deep basin range from 263.9 to 44,655.79 ppm, with an average of 4769.18 ppm (Figure 9). These results imply that (1) the slope and deep basin had a much higher primary productivity than the intra-platform basin during the Ediacaran–Cambrian transition stage in the study area, or (2) during this stage, the intra-platform basin was in anoxic condition.

Previous studies have shown that the silica content is positively correlated with the TOC content for the Early Cambrian Niutitang black shale, indicating the existence of Si_{bio} in this shale [17,76,77]. The fraction of the Si_{bio} content in the shale samples can be estimated as follows [78]:

$$Si_{bio} = Si_{total} - [Al_{total} \times (Si/Al)_{terrigenous}],$$

where Si_{total} is the total amount of silica in the sample, ppm; Al_{total} is the total amount of aluminum in the sample; and $(Si/Al)_{terrigenous}$ is the average Si/Al ratio of the upper crust.

The Si_{bio} contents of the shale samples analyzed in this study range from 0.17% to 94.44% (Figure 9). It should be noted that the samples of the slope and deep basin regions have much higher Si_{bio} contents (average of 27.52%) than those of the intra-platform basin (average of 18.08%), which indicates that the slope and deep basin environments had a higher productivity than the intra-platform basin. This conclusion is further verified by the Ni+Cu+Zn contents. As shown in Figure 9A–C, the Ni+Cu+Zn concentrations of the shale samples from the intra-platform basin region (85.11–881.34 ppm, average of 324.84 ppm) are lower than those from the slope and deep basin regions (36.97–4415.29 ppm, average of 415.55 ppm) (Figure 9D,E).

Phosphorous (P) is one of the essential nutrient elements for the growth of marine organisms on both short and long timescales, and its concentration in sediments has been used as an indicator of paleoproductivity [79,80]. In the studied shale samples, the P contents are 0.015–0.77% (Figures 9 and 10), which are higher than the content in the crust (700 ppm). These results suggest that the Upper Yangtze Region was a productive and dynamic region during the deposition stage of the Early Cambrian Niutitang black shale. As shown in Figure 10, there is a moderate correlation between P and TOC ($R^2 = 0.32$, n = 109), and this phenomenon probably indicates that during the deposition of this black shale, the primary productivity was high, which controlled the organic matter production.

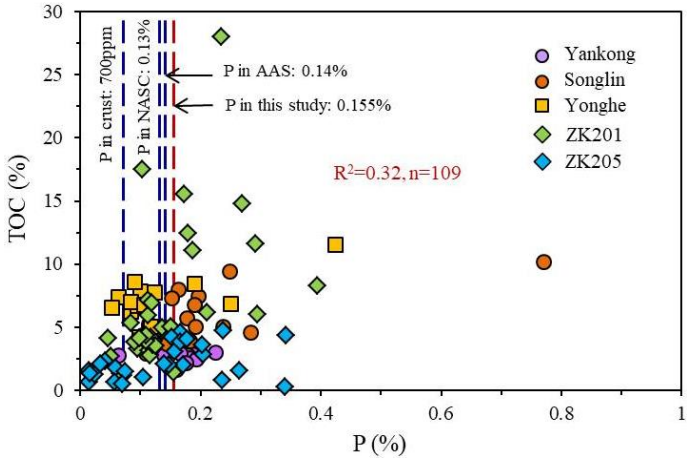


Figure 10. Plot of TOC versus P. The blue and red dotted lines indicate the average P contents of the different materials. NASC—North American Shale Composite; AAS—Average Archean Shale.

5.5. Paleoredox Conditions

The preservation of organic matter is mainly controlled by the redox conditions. In general, anoxic and euxinic conditions are beneficial for the preservation of organic matter [81–83]. The redox conditions during sedimentation can be indicated by single redox-sensitive elements (such as V, Mo, Ni, Re, U, Ce, and Eu) and the ratios of two different elements (mainly including U/Th, U/Mo, Re/Mo, V/(V + Ni), V/Cr, V/Sc, and Ni/Co). However, no single proxy can conclusively indicate the redox conditions because the distribution of these elements is affected by various factors [64,78,84,85]. In this study, indicators including U/Th, V/(V + Ni), V/Cr, and Ni/Co ratios and the V+Mo+U and δCe values, were adopted to analyze the paleo-sedimentary conditions of the Early Cambrian Niutitang black shale. The δCe value can be calculated using the following formula:

$$\delta Ce = 3 \times Ce_{sample}/(2 \times La_{sample} + Nd_{sample})$$

where Ce_{sample}, La_{sample}, and Nd_{sample} are the Ce, La, and Nd concentrations, respectively, of the shale samples [86].

Uranium (U) and V are redox-sensitive elements, and they are generally enriched under anoxic and euxinic conditions [64]. Cr and Th, unlike U and V, are not redox-sensitive elements and remain insoluble in the marine environment [78]. Therefore, the U/Th and V/Cr ratios can indicate oceanic redox conditions. Generally, U/Th > 1.25 represents anoxic conditions, and ratios as low as 0.75 represent strongly oxidizing conditions [87]. For V/Cr, >4.25 indicates anoxic conditions, 4.25–2 indicates suboxic conditions, and <2 indicates oxic conditions [81]. The V/(V + Ni) and Ni/Co ratios can also indicate redox conditions. It is widely accepted that both V/(V + Ni) and Ni/Co increase from oxic [V/(V + Ni) < 0.45; Ni/Co < 5], through suboxic [0.45 < V/(V + Ni) < 0.6; 5 < Ni/Co < 7], to anoxic [0.6 < V/(V + Ni); 7 < Ni/Co] conditions [64,78,81,88,89]. In addition, δCe > −0.1 and <−0.1 indicate anoxic and oxic conditions, respectively [90]. Since V, Mo, and U are all enriched in sediments deposited under anoxic to euxinic conditions but are dissolved and transported by oceanic water under oxic conditions, the V+Mo+U content can be used to effectively evaluate the evolution of the paleoredox conditions.

As shown in Figure 9, the U/Th ratios of the shale samples from the intra-platform basin vary from 0.88 to 209.03 (Figure 9A–C), with an average of 17.54. In contrast, the shale samples from the slope and deep basin regions have slightly lower U/Th ratios of 0.35–129.85 (Figure 9D,E) (excluding an abnormal value of 509.24 from well ZK205), with an average of 8.59. These results imply that (1) the studied area was dominated by suboxic to anoxic environments and there may have been short oxygenation events in the slope region, and (2) the intra-platform basin experienced a much stronger reducibility than the slope during the sedimentation of the Early Cambrian Niutitag black shale. These two deductions are also supported by the V/(V + Ni) ratios. The V/(V + Ni) ratios of the intra-platform basin shale samples are 0.756–0.994 (average of 0.906), indicating anoxic or even euxinic conditions of sedimentation, while those of the slope and deep basin shale samples range from 0.483 to 0.973, with an average of 0.803, indicating deposition under suboxic to anoxic conditions. This is consistent with the conclusions of our recent work, which is based on the concentrations and enrichment factors of U, Mo, Ni, and V [18].

The Early Cambrian Niutitang black shale samples have δCe values of 0.19–1.78, which are much higher than −0.1, supporting the conclusion that this shale was deposited under anoxic conditions. However, the other indicators, including V/Cr (1.54–22.24 for intra-platform basin region, and 0.13–25.22 for the slope and deep basin regions) and Ni/Co (3.65–62.98 for the intra-platform basin, and 1.65–40.63 for slope and deep basin regions), indicate that the sedimentary environment of this shale fluctuated between oxic, suboxic, and anoxic (or even euxinic) (Figure 9). Previous studies constructed a stratified and fluctuating model for the oceanic water mass on the Yangtze Block during the Ediacaran–Cambrian transition stage, arguing that several oxygenation events occurred in the background of a generally anoxic environment [11,13,34].

Taking into account the numerous indicators used in this study, including U/Th, V/(V + Ni), V/Cr, Ni/Co, V+Mo+U, and δCe, we suggest that the Early Cambrian black shale in the Upper Yangtze Region was deposited under primarily anoxic conditions, with several short oxygenation events. In contrast to the slope setting, the water environment in the intra-platform basin setting was more anoxic. The reasons for this may include (1) that hydrothermal activities and upwelling events improved the oxygen concentration of the water in the slopesetting, and (2) the intra-platform basin was relatively restricted during the sedimentation of the Early Cambrian Niutitang black shale. In addition, the typomorphic characteristics of the pyrite are significantly different in the intra-platform basin and slope to deep basin regions. The pyrite is mainly framboids in the intra-platform basin, but there is a large amount of colloidal pyrite in the slope to deep basin (Figure 11), implying a euxinic condition in the intra-platform basin [91,92].

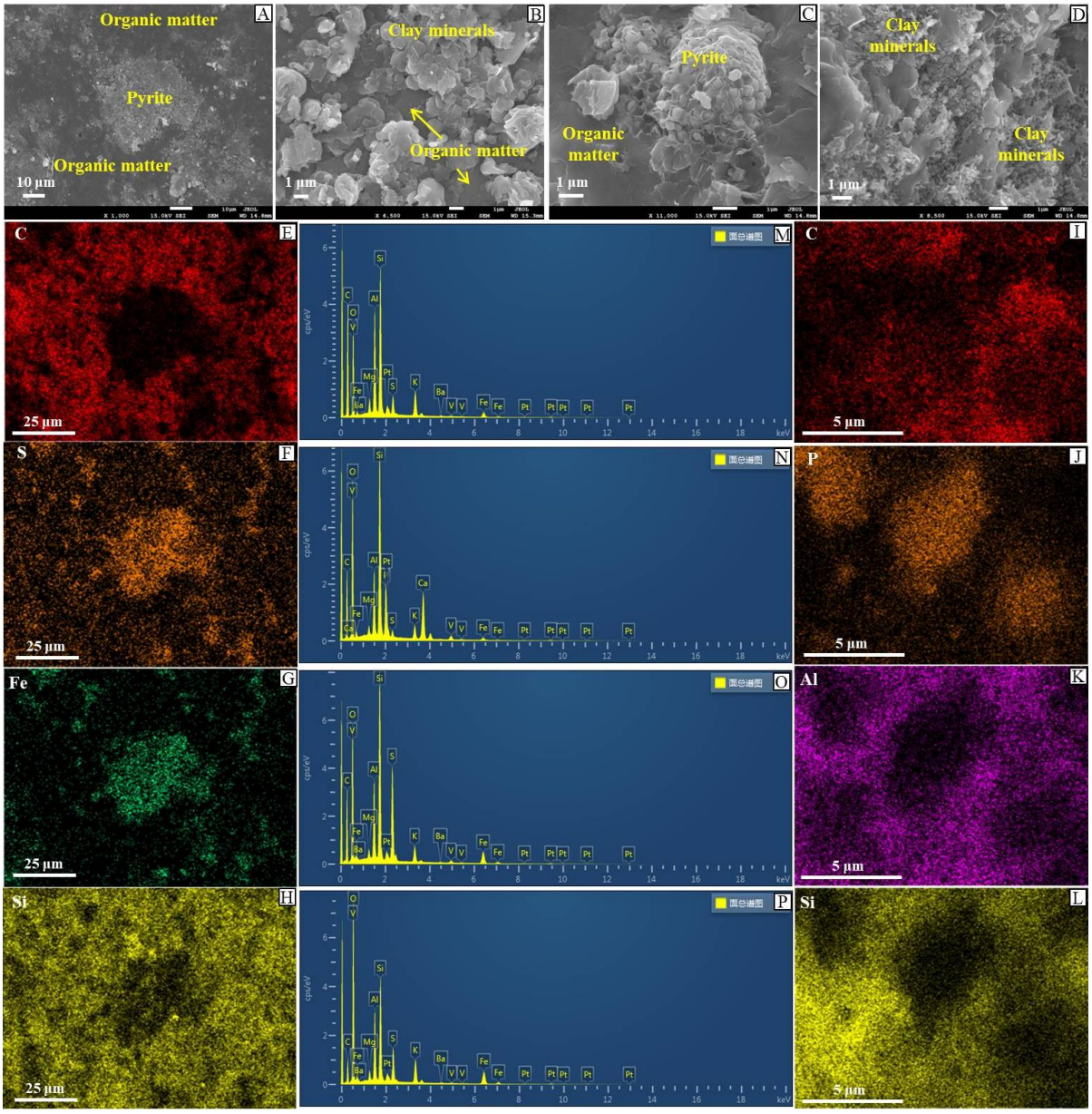


Figure 11. SEM images of the Early Cambrian black shale. (**A**,**B**) Samples from well ZK102; (**C**,**D**) sample from the Songlin section; (**E**–**H**) distributions of C, S, Fe, and Si corresponding to subgraph A; (**I**–**L**) distributions of C, P, Al, and Si corresponding to subgraph D; (**M**–**P**) energy spectra of subgraphs (**A**–**D**), respectively.

5.6. Water Mass Restriction

The degree of water mass restriction affects the sedimentary environment and the geochemical cycle, and it is a significant feature of marine systems [85]. The trace elements U and Mo can be combined to evaluate water mass restriction because (1) both of these elements have long retention times in seawater, and thus exhibit global seawater concentrations; (2) both of these elements exist in high valence states (U^{+6} and Mo^{+6}) under oxic conditions and are enriched in sediments in low valence state forms (U^{+4} and Mo^{+4}) under anoxic conditions; (3) the sediments absorb U earlier than Mo in unrestricted water masses; and (4) the absorption rate of Mo by sediments is faster than that of U in weakly and strongly restricted water masses [93–95]. Thus, a plot of U_{ef} versus Mo_{ef} can be used to evaluate the degree of water mass restriction. In addition, the supply of Mo to the basin decreases with increasing water mass restriction, resulting in low Mo/TOC ratios in a strongly restricted basin [96]. In this study, the U_{ef}-Mo_{ef} and Mo-TOC diagrams were combined to evaluate the degree of water mass restriction during the deposition of the Early Cambrian black shale in the Upper Yangtze Region.

As shown in Figure 12A, the Mo/TOC ratios of the shale samples from the intra-platform basin range from 0.37×10^{-4} to 29.74×10^{-4}, while the ratios of the slope and deep basin shale samples vary from 0.19×10^{-4} to 94×10^{-4}, suggesting that (1) the intra-platform basin was more restricted than the deep basin, and (2) the water mass restriction of the slope and deep basin regions changed more frequently than that of the intra-platform basin during the deposition of the Early Cambrian Niutitang black shale.

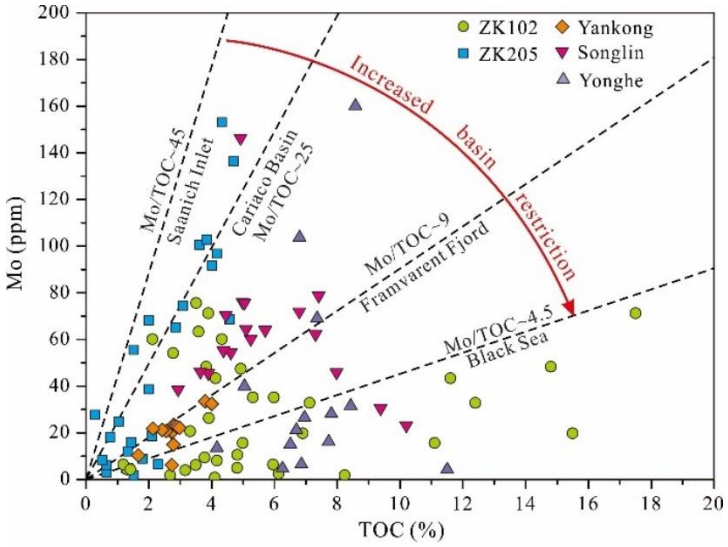


Figure 12. Plots of TOC versus Mo (modified from [94]).

5.7. Controls on Organic Matter Accumulation

The Yangtze Block experienced intense extension and block tilting, leading to the development of an intra-platform basin on the paleohigh surrounded by a large-scale open siliceous deep basin. As a result, during the terminal Ediacaran–earliest Cambrian stage of the Yangtze Block, the intra-platform basin, slope, and deep basin sedimentary setting belts were distributed from northwest to southeast (Figure 1) [14,32,47]. During this stage, upwelling events brought a large amount of nutrients to the shallow water regions, resulting in the phytoplankton in the shallow water flourishing [14,26]. In addition, organisms such as worms, sponges, and bacteria exploded around the hydrothermal centers (especially the large faults in the slope region) [26,53]. As a result, the intra-platform basin margins and slope had significantly higher primary productivities than the inner intra-platform basin (Figure 9).

Based on their profiles, the Yonghe section and ZK102 and ZK205 wells are all distributed in areas with relatively high primary productivities (see Section 5.4), and the

organic matter content decreases from the Yonghe section, through well ZK102, to well ZK205. These results suggest that the organic matter accumulation was mainly controlled by the paleoproductivity in areas of high primary productivity. In these areas, the high paleoproductivity generated a large amount of organic matter, part of which was oxidized and the rest of which was diluted (Figure 13). The combined effects of the high primary productivity, sedimentation rate, and suboxic-anoxic conditions are supported by the results of the correlation analysis of the TOC content and various geochemical proxies. Taking well ZK102 as an example, none of the proxies have a correlation coefficient greater than 0.26 with the TOC content (Figure 14).

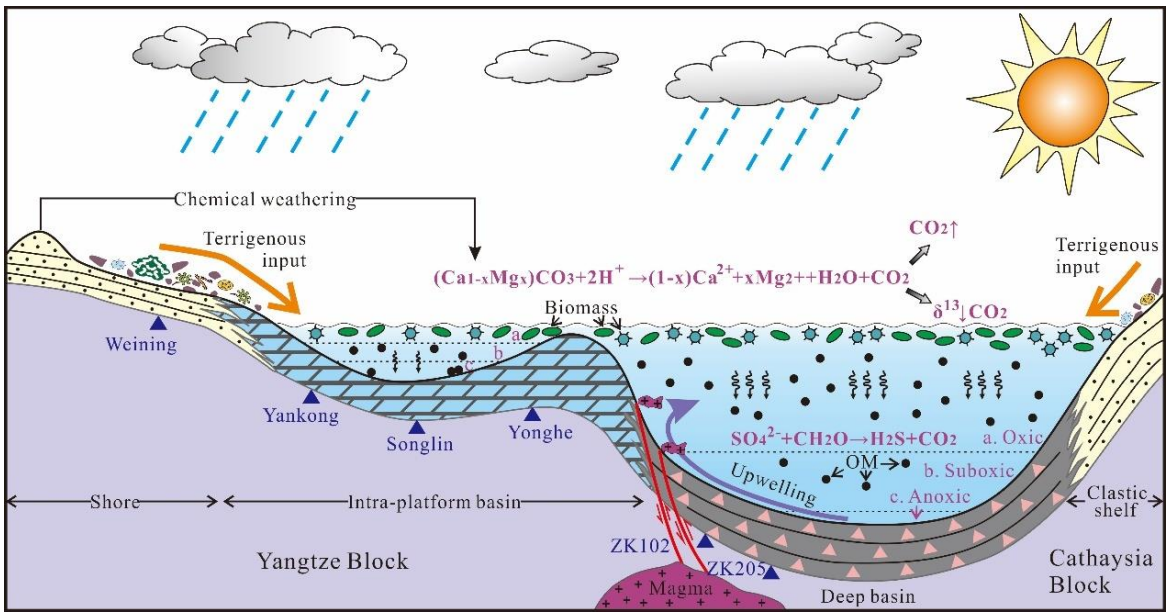


Figure 13. Schematic sketch illustrating the organic matter accumulation mechanism in the Upper Yangtze region during the deposition of the Early Cambrian black shale.

	U/Th	V/(V+Ni)	V/Cr	Ni/Co	δCe	δEu	V+Mo+U	Babio	P	Si bio	Ni+Cu+Zn	∑REE	La/Lu	Sr/Ba	Y/Ho	Al/Ti	TOC
U/Th	1.00	0.38	0.78	0.68	−0.17	0.27	0.82	−0.46	0.19	0.13	0.00	−0.24	0.24	−0.29	−0.74	0.11	0.44
V/(V+Ni)		1.00	0.57	0.89	−0.40	0.58	0.55	0.19	−0.52	0.80	−0.69	−0.34	0.65	−0.38	−0.12	−0.65	0.64
V/Cr			1.00	0.80	−0.06	0.33	0.98	−0.50	0.24	0.18	−0.12	−0.43	0.10	−0.30	−0.72	0.14	0.53
Ni/Co				1.00	−0.35	0.57	0.78	−0.07	−0.33	0.69	−0.58	−0.41	0.59	−0.34	−0.45	−0.34	0.69
δCe					1.00	−0.13	−0.02	−0.26	0.57	−0.57	0.50	−0.08	−0.45	−0.19	0.00	0.32	−0.21
δEu						1.00	0.30	0.45	−0.36	0.71	−0.66	−0.77	0.39	−0.38	−0.13	−0.52	0.80
V+Mo+U							1.00	−0.53	0.28	0.14	−0.04	−0.38	0.12	−0.38	−0.70	0.12	0.55
Babio								1.00	−0.69	0.57	−0.66	−0.09	0.33	0.23	0.55	−0.59	0.19
P									1.00	−0.75	0.80	0.14	−0.55	−0.01	−0.42	0.68	−0.19
Si bio										1.00	−0.88	−0.33	0.76	−0.17	0.07	−0.76	0.65
Ni+Cu+Zn											1.00	0.33	−0.59	−0.16	−0.04	0.53	−0.39
∑REE												1.00	0.18	0.50	0.18	0.24	−0.60
La/Lu													1.00	−0.12	0.01	−0.54	0.44
Sr/Ba			Yankong section											1.00	−0.04	0.48	−0.59
Y/Ho															1.00	−0.46	−0.19
Al/Ti																1.00	−0.51
TOC																	1.00

	U/Th	V/(V+Ni)	V/Cr	Ni/Co	δCe	δEu	V+Mo+U	Babio	P	Si bio	Ni+Cu+Zn	∑REE	La/Lu	Sr/Ba	Y/Ho	Al/Ti	TOC
U/Th	1.00	−0.06	0.21	0.02	0.51	0.80	0.17	0.54	−0.01	−0.04	0.35	−0.52	−0.54	−0.46	−0.38	0.01	0.26
V/(V+Ni)		1.00	0.35	0.67	−0.33	0.00	0.50	−0.17	−0.15	0.54	0.25	−0.24	−0.11	−0.21	−0.11	0.20	0.05
V/Cr			1.00	0.49	0.13	0.19	0.96	0.38	0.11	−0.15	0.77	−0.26	−0.41	−0.34	−0.41	0.04	0.20
Ni/Co				1.00	−0.42	0.18	0.60	−0.13	0.05	0.37	0.28	−0.37	−0.35	−0.29	−0.39	0.47	−0.16
δCe					1.00	0.37	0.03	0.58	0.04	−0.59	0.24	−0.02	−0.03	0.04	−0.27	−0.17	0.08
δEu						1.00	0.18	0.51	−0.11	−0.14	0.34	−0.64	−0.58	−0.44	−0.55	0.27	−0.10
V+Mo+U							1.00	0.28	0.08	−0.01	0.79	−0.33	−0.45	−0.40	−0.37	0.14	0.14
Babio								1.00	0.17	−0.37	0.46	−0.23	−0.33	−0.35	−0.20	−0.13	0.17
P									1.00	0.03	0.04	0.01	−0.05	−0.09	0.13	0.13	−0.13
Si bio										1.00	−0.13	−0.25	−0.15	−0.19	0.27	0.25	0.08
Ni+Cu+Zn											1.00	−0.46	−0.56	−0.59	−0.33	0.16	0.17
∑REE												1.00	0.81	0.74	0.38	−0.40	−0.04
La/Lu													1.00	0.81	0.44	−0.32	−0.10
Sr/Ba			ZK102 well											1.00	0.35	−0.26	−0.18
Y/Ho															1.00	−0.39	0.26
Al/Ti																1.00	−0.49
TOC																	1.00

Figure 14. Correlation coefficients of TOC content with various geochemical proxies (Purple mean positive correlation, and blue mean negative correlation).

As was discussed in Section 5.4, the inner part of the intra-platform basin (Yankong and Songlin sections) had a lower primary productivity than the slope (well ZK102), deep

basin (well ZK205), and the margins of the intra-platform basin (Yonghe section) (Figure 9), indicating that the amount of initial organic matter on the inner intra-platform basin was low during the deposition of the Early Cambrian Niutitang black shale. Thus, the anoxic conditions of the marine water were necessary for the accumulation and preservation of the organic matter. As shown in Figure 2, the Songlin section has a much higher TOC content than the Yankong section, which may be because the former section experienced more anoxic conditions than the latter during the deposition of the Early Cambrian Niutitang black shale (Figures 9 and 11). In addition, the TOC contents of the Yankong section are positively correlated with the geochemical redox proxies (Figure 14), which indicates that the organic matter accumulation and enrichment in the intra-platform basin setting were controlled by the preservation conditions (Figures 9 and 13). In this study, we could not definitively conclude whether a preservation model or a productivity model was best for the Early Cambrian Niutitang black shale in the Upper Yangtze Region based on only five profiles. However, the distributions of the geochemical proxies and the TOC contents indicate that the mechanisms of the organic matter accumulation were different in the intra-platform basin setting compared to the slope to deep basin settings.

6. Conclusions

(1) For the Early Cambrian Niutitang black shale in the Upper Yangtze Region, geochemical proxies were used to compare the paleoenvironments and the mechanisms of organic matter accumulation in this shale in the intra-platform basin, slope, and deep basin settings. In contrast to the slope and deep basin settings, the intra-platform setting had a significantly higher terrigenous input and was deposited under more restricted conditions. Hydrothermal activities and upwelling events supplied a large amount of nutrients and metal elements to the surface layer of the sediments during the sedimentation of the Early Cambrian Niutitang black shale, especially in the slope and intra-platform basin margin settings.

(2) The redox proxies, mainly including U/Th, V/(V + Ni), V/Cr, V+Mo+U, and δCe, indicate that the black shale studied was deposited under suboxic-anoxic conditions. The intra-platform basin was more anoxic than the slope setting. The primary productivity was higher in the slope and deep basin settings than in the intra-platform basin. For the intra-platform basin setting, its inner part had a low productivity, but the productivity was high on its margins.

(3) In the slope and deep basin settings, the high paleoproductivity generated a large amount of organic matter, and its preservation was affected by the redox conditions. The redox conditions were the most significant factor controlling the preservation of the organic matter in the inner intra-platform basin because the paleoproductivity was lower than that in the intra-platform basin margins, slope, and deep basin settings. The intra-platform basin margins were the most favorable areas for preserving organic matter because these areas had a high paleoproductivity and anoxic conditions.

Supplementary Materials: The following supporting information can be downloaded at: https://www.mdpi.com/article/10.3390/en15134551/s1.

Author Contributions: P.X., data curation, formal analysis, and writing of the original draft. F.H., conceptualization and supervision. J.T., supervision and writing—review & editing. W.Z., sample collection and experiments. Y.F., methodology and supervision. C.G., writing—review & editing. Z.Y., writing—review & editing. K.L., writing—review & editing. K.W., writing—review & editing. All authors have read and agreed to the published version of the manuscript.

Funding: This work was financially supported by the National Natural Science Fund of China (Grant Nos. 42002166, 42162016, and 41690134) and the Guizhou Provincial Fund Project (Grant Nos. [2020]1Y161, [2020]1Y166, ZK[2021]199, ZK[2022]YIBAN106, and ZK[2022]YIBAN213).

Institutional Review Board Statement: Not applicable.

Informed Consent Statement: Not applicable.

Data Availability Statement: Available from corresponding author.

Conflicts of Interest: The authors declare no conflict of interest.

References

1. Fan, D.; Zhang, T.; Ye, J. *Black Rock Series and Related Deposits in China*; Science Press: Beijing, China, 2004.
2. Wang, Z.W.; Fu, X.G.; Feng, X.L.; Song, C.Y.; Wang, D.; Chen, W.B.; Zeng, S.Q. Geochemical features of the black shales from the Wuyu Basin, southern Tibet: Implications for palaeoenvironment and palaeoclimate. *Geol. J.* **2017**, *52*, 282–297. [CrossRef]
3. Shi, C.H.; Cao, J.; Han, S.C.; Hu, K.; Bian, L.Z.; Yao, S.P. A review of polymetallic mineralization in lower Cambrian black shales in South China: Combined effects of seawater, hydrothermal fluids, and biological activity. *Palaeogeogr. Palaeoclimatol. Palaeoecol.* **2021**, *561*, 110073. [CrossRef]
4. Zou, C.N.; Zhao, Q.; Cong, L.Z.; Wang, H.Y.; Shi, Z.S.; Wu, J.; Pan, S.Q. Development progress, potential and prospect of shale gas in China. *Nat. Gas Ind.* **2021**, *41*, 1–14, (In Chinese with English abstract).
5. Guizhou Geological Survey. In *Regional Geology of China*; Geology Press: Beijing, China, 2017.
6. Fu, Y.; Xia, P.; Long, Z.; Zhang, G.J.; Qiao, W.L.; Guo, C.; Yang, Z. Continental weathering of Yangtze area during Ediacaran (Sinian)–Cambrian transition stage: Advances and prospects. *Geol. Rev.* **2021**, *67*, 1–18, (In Chinese with English abstract).
7. Zhu, L.J.; Zhang, D.W.; Zhang, J.C.; Wang, G.L.; Yang, T.B.; Chen, H.G. *Geological Theroy and Practice of Shale Gas in Paleozoic Passive Continental Margin, Eastern of Upper Yangtze*; Science Press: Beijing, China, 2019.
8. Zou, C.N.; Yang, Z.; Dong, D.Z.; Zhao, Q.; Chen, Z.H.; Feng, Y.L.; Li, J.R.; Wang, X.N. Formation, Distribution and Prospect of Unconventional Hydrocarbons in Source Rock Strata in China. *Earth Sci.* **2022**, *47*, 1517–1533, (In Chinese with English abstract).
9. Hao, F.; Zou, H.Y. Cause of shale gas geochemical anomalies and mechanisms for gas enrichment and depletion in high-maturity shales. *Mar. Pet. Geol.* **2013**, *44*, 1–12. [CrossRef]
10. Zhang, K.; Song, Y.; Jia, C.Z.; Jiang, Z.X.; Han, F.L.; Wang, P.F.; Yuan, X.J.; Yang, Y.M.; Zeng, Y.; Li, Y.; et al. Formation mechanism of the sealing capacity of the roof and floor strata of marine organic-rich shale and shale itself, and its influence on the characteristics of shale gas and organic matter pore development. *Mar. Pet. Geol.* **2022**, *140*, 105647. [CrossRef]
11. Li, C.; Love, G.D.; Lyons, T.W.; Fike, D.A.; Sessions, A.L.; Chu, X.L. A Stratified Redox Model for the Ediacaran Ocean. *Science* **2010**, *328*, 80–83. [CrossRef]
12. Li, C.; Zhang, Z.H.; Jin, C.S.; Cheng, M.; Wang, H.Y.; Huang, J.H.; Algeo, T.J. Spatiotemporal evolution and causes of marine euxinia in the early Cambrian Nanhua Basin (South China). *Palaeogeogr. Palaeoclimatol. Palaeoecol.* **2020**, *546*, 109676. [CrossRef]
13. Jin, C.S.; Li, C.; Algeo, T.J.; Planavsky, N.J.; Cui, H.; Yang, X.L.; Zhao, Y.L.; Zhang, X.L.; Xie, S.C. A highly redox–heterogeneous ocean in South China during the early Cambrian (~529–514 Ma): Implications for biota–environment co–evolution. *Earth Planet. Sci. Lett.* **2016**, *441*, 38–51. [CrossRef]
14. Yeasmin, R.; Chen, D.Z.; Fu, Y.; Wang, J.G.; Guo, Z.H.; Guo, C. Climatic–oceanic forcing on the organic accumulation across the shelf during the Early Cambrian (Age 2 through 3) in the mid–upper Yangtze Block, NE Guizhou, South China. *J. Asian Earth Sci.* **2017**, *134*, 365–386. [CrossRef]
15. Zhou, W.X. *Sedimentary Environment and Geochemical Characteristics of the Lower Cambrian Black Rock Series in Northern Guizhou*; Guizhou University: Guiyang, China, 2017.
16. Zhai, L.N.; Wu, C.D.; Ye, Y.T.; Zhang, S.C.; Wang, Y.Z. Fluctuations in chemical weathering on the Yangtze Block during the Ediacaran–Cambrian transition: Implications for paleoclimatic conditions and the marine carbon cycle. *Palaeogeogr. Palaeoclimatol. Palaeoecol.* **2018**, *490*, 280–292. [CrossRef]
17. Xia, P.; Li, H.N.; Fu, Y.; Qiao, W.L.; Guo, C.; Yang, Z.; Huang, J.Q.; Mou, Y.L. Effect of lithofacies on pore structure of the Cambrian organic–rich shale in northern Guizhou, China. *Geol. J.* **2021**, *56*, 1130–1142. [CrossRef]
18. Fu, Y.; Zhou, W.X.; Wang, H.J.; Qiao, W.L.; Ye, Y.T.; Jiang, R.; Wang, X.M.; Su, J.; Li, D.; Xia, P. The relationship between environment and geochemical characteristics of black rock series of Lower Cambrian in northern Guizhou. *Acta Geol. Sin.* **2021**, *95*, 536–5483, (In Chinese with English abstract).
19. Kuypers, M.M.M.; Pancost, R.D.; Nijenhuis, I.A.; Sinninghe Damste, J.S. Enhanced productivity led to increased organic carbon burial in the euxinic North Atlantic basin during the late Cenomanian oceanic anoxic event. *Paleoceanography* **2002**, *17*, 1051. [CrossRef]
20. Hartnett, H.E.; Devol, A.H. Role of a strong oxygen–deficient zone in the preservation and degradation of organic matter: A carbon budget for the continental margins of northwest Mexico and Washington State. *Geochim. Cosmochim. Acta* **2003**, *67*, 247–264. [CrossRef]
21. Ding, X.J.; Liu, G.D.; Huang, Z.L.; Lu, X.J.; Chen, Z.L.; Gu, F. Controlling function of organic matter supply and preservation on formation of source rock. *Earth Sci.* **2016**, *41*, 832–842. (In Chinese with English abstract)
22. Pedersen, T.F.; Calvert, S.E. Anoxia vs. Productivity: What Controls the Formation of Organic–Carbon–Rich Sediments and Sedimentary Rocks? *AAPG Bull.* **1990**, *74*, 454–466.
23. Tyson, R.V. Sedimentation rate, dilution, preservation and total organic carbon: Some results of a modelling study. *Org. Geochem.* **2001**, *32*, 333–339. [CrossRef]
24. Tyson, R.V.; Harris, N.B. *The "Productivity Versus Preservation" Controversy: Cause, Flaws, and Resolution, The Deposition of Organic–Carbon–Rich Sediments: Models, Mechanisms, and Consequences*; SEPM Special Publication: Tulsa, OK, USA, 2005.

25. Lu, Y.B.; Jiang, S.; Lu, Y.C.; Xu, S.; Shu, Y.; Wang, Y.X. Productivity or preservation? The factors controlling the organic matter accumulation in the late Katian through Hirnantian Wufeng organic–rich shale, South China. *Mar. Pet. Geol.* **2019**, *109*, 22–35. [CrossRef]
26. Xia, P.; Fu, Y.; Yang, Z.; Guo, C.; Huang, J.Q.; Huang, M.Y. The relationship between sedimentary environment and organic matter accumulation in the Niutitang black shale in Zhenyuan, northern Guizhou. *Acta Geol. Sin.* **2020**, *94*, 947–956. (In Chinese with English abstract)
27. Algeo, T.J.; Maynard, J.B. Trace-element behavior and redox facies in core shales of Upper Pennsylvanian Kansas-type cyclothems. *Chem. Geol.* **2004**, *206*, 289–318. [CrossRef]
28. Li, J. *Study on Paleo-Environmental Reconstruction and Organic Matter Accumulation of the Lower Cambrian Niutitang Formation in Northern Guizhou*; China University of Geosciences: Beijing, China, 2018.
29. Wei, H.R.; Yang, R.D.; Gao, J.B.; Chen, J.Y.; Liu, K.; Cheng, W. New Evidence for Hydrothermal Sedimentary Genesis of the Ni–Mo Deposits in Black Rock Series of the Basal Cambrian, Guizhou Province: Discovery of Coarse–Grained Limestones and its Geochemical Characteristics. *Acta Geol. Sin.* **2012**, *86*, 51–61.
30. Liu, Z.H.; Zhuang, X.G.; Teng, G.E.; Xie, X.M.; Yin, L.M.; Bian, L.Z.; Feng, Q.L.; Algeo, T.J. The lower cambrian niutitang formation at yangtiao (guizhou, sw china): Organic matter enrichment, source rock potential, and hydrothermal influences. *J. Pet. Geol.* **2015**, *38*, 411–432. [CrossRef]
31. Wang, N.; Li, M.J.; Tian, X.W.; Hong, H.T.; Liu, P.; Chen, G.; Wang, M.L. Main factors controlling the organic matter enrichment in the Lower Cambrian sediments of the Sichuan Basin, SW China. *Geol. J.* **2019**, *55*, 3083–3096. [CrossRef]
32. Chen, D.Z.; Wang, J.G.; Qing, H.R.; Yan, D.T.; Li, R.W. Hydrothermal venting activities in the Early Cambrian, South China: Petrological, geochronological and stable isotopic constraints. *Chem. Geol.* **2009**, *258*, 168–181. [CrossRef]
33. Jia, Z.B.; Hou, D.J.; Sun, D.Q.; Jiang, Y.H.; Zhao, Z.; Zhang, Z.M.; Hong, M.; Chang, Z.; Dong, L.C. Characteristics and geological implications of rare earth elements in black shale in hydrothermal sedimentation areas: A case study from the Lower Cambrian Niutitang Fm shale in central and eastern Guizhou. *Nat. Gas Ind.* **2018**, *38*, 44–51. (In Chinese with English abstract)
34. Li, C.; Shi, W.; Cheng, M.; Jin, C.S.; Algeo, T.J. The redox structure of Ediacaran and early Cambrian oceans and its controls. *Sci. Bull.* **2020**, *65*, 2141–2149. [CrossRef]
35. Awan, R.S.; Liu, C.L.; Gong, H.W.; Dun, C.; Tong, C.; Chamssidini, L.G. Paleo-sedimentary environment in relation to enrichment of organic matter of Early Cambrian black rocks of Niutitang Formation from Xiangxi area China. *Mar. Pet. Geol.* **2020**, *112*, 104057. [CrossRef]
36. Wu, Y.W.; Tian, H.; Gong, D.J.; Li, T.F.; Zhou, Q. Paleo-environmental variation and its control on organic matter enrichment of black shales from shallow shelf to slope regions on the Upper Yangtze Platform during Cambrian Stage 3. *Palaeogeogr. Palaeoclimatol. Palaeoecol.* **2020**, *545*, 109653. [CrossRef]
37. Gao, Z.Y.; Liang, Z.; Hu, Q.H.; Jiang, Z.X.; Xuan, Q.X. A new and integrated imaging and compositional method to investigate the contributions of organic matter and inorganic minerals to the pore spaces of lacustrine shale in China. *Mar. Pet. Geol.* **2021**, *127*, 104962. [CrossRef]
38. Ning, S.T.; Xia, P.; Hao, F.; Tian, J.Q.; Zhong, Y.; Zou, N.N.; Fu, Y. Shale facies and its relationship with sedimentary environment and organic matter of Niutitang black shale, Guizhou Province. *Nat. Gas Geosci.* **2021**, *32*, 1297–1307.
39. Dai, C.G.; Zheng, Q.Q.; Chen, J.S.; Wang, M.; Zhang, H. The metallogenic geological background of the Xuefeng-Caledonian tectonic cycle in Guizhou, China. *Earth Sci. Front.* **2013**, *20*, 219–225.
40. Shu, L.S. An analysis of principal features of tectonic evolution in South China Block. *Geol. Bull. China* **2012**, *31*, 1035–1053. (In Chinese with English abstract)
41. Charvet, J. The Neoproterozoic-Early Paleozoic tectonic evolution of the South China Block: An overview. *J. Asian Earth Sci.* **2013**, *74*, 198–209. [CrossRef]
42. Wang, J.; Li, Z.X. History of Neoproterozoic rift basins in South China: Implications for Rodinia break–up. *Precambrian Res.* **2003**, *122*, 141–158. [CrossRef]
43. Wang, X.Q.; Shi, X.Y.; Jiang, G.Q.; Zhang, W.H. New U-Pb age from the basal Niutitang Formation in South China: Implications for diachronous development and condensation of stratigraphic units across the Yangtze platform at the Ediacaran-Cambrian transition. *J. Asian Earth Sci.* **2012**, *48*, 1–8. [CrossRef]
44. Zhu, M.Y.; Zhang, J.M.; Yang, A.H.; Li, G.; Steiner, M.; Erdtmann, B.D. Sinian-Cambrian stratigraphic framework for shallow-to deep-water environments of the Yangtze Platform: An integrated approach. *Prog. Nat. Sci.* **2003**, *13*, 951–960. [CrossRef]
45. Lehmann, B.; Frei, R.; Xu, L.G.; Mao, J.W. Early Cambrian Black Shale-Hosted Mo-Ni and V Mineralization on the Rifted Margin of the Yangtze Platform, China: Reconnaissance Chromium Isotope Data and a Refined Metallogenic Model. *Econ. Geol.* **2016**, *111*, 89–103. [CrossRef]
46. Xu, L.G.; Mao, J.W. Trace element and C-S-Fe geochemistry of Early Cambrian black shales and associated polymetallic Ni-Mo sulfide and vanadium mineralization, South China: Implications for paleoceanic redox variation. *Ore Geol. Rev.* **2021**, *135*, 104210. [CrossRef]
47. Wang, J.G.; Chen, D.Z.; Wang, D.; Yan, D.T.; Zhou, X.Q.; Wang, Q.C. Petrology and geochemistry of chert on the marginal zone of Yangtze Platform, western Hunan, South China, during the Ediacaran-Cambrian transition. *Sedimentology* **2012**, *59*, 809–829. [CrossRef]

48. Xu, L.G.; Lehmann, B.; Mao, J.W.; Qu, W.J.; Du, A.D. Re-Os age of polymetallic Ni-Mo-PGE-Au mineralization in Early Cambrian black shales of South China-A reassessment. *Econ. Geol.* **2011**, *106*, 511–522.
49. Chen, D.Z.; Zhou, X.Q.; Fu, Y.; Wang, J.G.; Yan, D.T. New U–Pb zircon ages of the Ediacaran-Cambrian boundary strata in South China. *Terra Nova* **2015**, *27*, 62–68. [CrossRef]
50. Mclennan, S.M. Relationships between the trace element composition of sedimentary rocks and upper continental crust. *Geochem. Geophys. Geosystems* **2001**, *2*, 2000GC000109. [CrossRef]
51. Gromet, L.P.; Haskin, L.A.; Korotev, R.L. The "North American shale composite": Its compilation, major and trace element characteristics. *Geochim. Et Cosmochim. Acta* **1984**, *48*, 2469–2482. [CrossRef]
52. Usui, A.; Someya, M. Distribution and composition of marine hydrogenetic and hydrothermal manganese deposits in the northwest Pacific. *Geol. Soc. Lond. Spec. Publ.* **1997**, *119*, 177–198. [CrossRef]
53. Jia, Z.B.; Hou, D.J.; Sun, D.Q.; Huang, Y.X. Hydrothermal sedimentary discrimination criteria and its coupling relationship with the source rock. *Nat. Gas Geosci.* **2016**, *27*, 1025–1034, (In Chinese with English abstract).
54. Zhang, K.; Liu, R.; Liu, Z.J.; Li, L.; Wu, X.P.; Zhao, K.A. Influence of palaeoclimate and hydrothermal activity on organic matter accumulation in lacustrine black shales from the Lower Cretaceous Bayingebi Formation of the Yin'e Basin, China. *Palaeogeogr. Palaeoclimatol. Palaeoecol.* **2020**, *560*, 110007.
55. Yuan, W.; Liu, G.; Bulseco, A.; Xu, L.G.; Zhou, X.X. Controls on U enrichment in organic–rich shales from the Triassic Yanchang Formation, Ordos Basin, Northern China. *J. Asian Earth Sci.* **2021**, *212*, 104735. [CrossRef]
56. Zhu, G.Y.; Wang, P.J.; Li, T.T.; Zhao, K.; Zheng, W.; Feng, X.B.; Shen, J.; Grasby, S.E.; Sun, G.Y.; Tang, S.L.; et al. Mercury record of intense hydrothermal activity during the early Cambrian, South China. *Palaeogeogr. Palaeoclimatol. Palaeoecol.* **2021**, *568*, 110294. [CrossRef]
57. Wei, S.C.; Chen, Q.F.; Fu, Y.; Cui, T.; Liang, H.P.; Ge, Z.H.; Zhang, P.; Zhang, Y. Origin of Cherts during the Ediacaran-Cambrian Transition in Hunan and Guizhou Provinces, China: Evidences from REE and Ge/Si. *Acta Sci. Nat. Univ. Pekin.* **2018**, *54*, 1010–1020. (In Chinese with English abstract)
58. Ruhlin, D.E.; Owen, R.M. The rare earth element geochemistry of hydrothermal sediments from the East Pacific Rise: Examination of a seawater scavenging mechanism. *Geochim. Et Cosmochim. Acta* **1986**, *50*, 393–400. [CrossRef]
59. Nesbitt, H.W.; Young, G.M. Early Proterozoic climates and plate motions inferred from major element chemistry of lutites. *Nature* **1982**, *299*, 715–717. [CrossRef]
60. Nesbitt, H.W.; Young, G.M. Formation and Diagenesis of Weathering Profiles. *J. Geol.* **1989**, *97*, 129–147. [CrossRef]
61. Mclennan, S.M. Weathering and Global Denudation. *J. Geol.* **1993**, *101*, 295–303. [CrossRef]
62. Fedo, C.M.; Wayne Nesbitt, H.; Young, G.M. Unraveling the effects of potassium metasomatism in sedimentary rocks and paleosols, with implications for paleoweathering conditions and provenance. *Geology* **1995**, *23*, 921–924. [CrossRef]
63. Yao, W.H.; Li, Z.X.; Li, W.X. Was there a Cambrian ocean in South China?—Insight from detrital provenance analyses. *Geol. Mag.* **2015**, *152*, 184–191. [CrossRef]
64. Tribovillard, N.; Algeo, T.J.; Lyons, T.; Riboulleau, A. Trace metals as paleoredox and paleoproductivity proxies: An update. *Chem. Geol.* **2006**, *232*, 12–32. [CrossRef]
65. Rachold, V.; Brumsack, H.J. Inorganic geochemistry of Albian sediments from the Lower Saxony Basin NW Germany: Palaeoenvironmental constraints and orbital cycles. *Palaeogeogr. Palaeoclimatol. Palaeoecol.* **2001**, *174*, 121–143.
66. Wang, Z.G.; Yu, X.Y.; Zhao, Z.H. *Geochemistry of Rare Earth Elements*; Science Press: Beijing, China, 1989.
67. Wright, J.; Schrader, H.; Holser, W.T. dox variations in ancient oceans recorded by rare earth elements in fossil apatite. *Geochim. Cosmochim. Acta* **1987**, *51*, 631–644. [CrossRef]
68. Kechiched, R.; Laouar, R.; Bruguier, O.; Kocsis, L.; Salmi-Laouar, S.; Bosch, D.; Ameur-Zaimeche, O.; Foufou, A.; Larit, H. Comprehensive REE + Y and sensitive redox trace elements of Algerian phosphorites (Tébessa, eastern Algeria): A geochemical study and depositional environments tracking. *J. Geochem. Explor.* **2020**, *208*, 106396. [CrossRef]
69. Zhao, C.J.; Kang, Z.H.; Hou, Y.H.; Yu, X.D.; Wang, E.B. Geochemical characteristics of rare earth elements and their geological significance of Permian shales in Lower Yangtze Area. *Earth Sci.* **2020**, *45*, 4118–4127. (In Chinese with English abstract)
70. Schoepfer, S.D.; Shen, J.; Wei, H.Y.; Tyson, R.V.; Ingall, E.; Algeo, T.J. Total organic carbon, organic phosphorus, and biogenic barium fluxes as proxies for paleomarine productivity. *Earth Sci. Rev.* **2015**, *149*, 23–52. [CrossRef]
71. Moore, J.K.; Fu, W.W.; Primean, F.; Britten, G.L.; Lindsay, K.; Long, M.; Doney, S.C.; Mahowald, N.; Hoffman, F.; Randerson, J.T. Sustained climate warming drives declining marine biological productivity. *Science* **2018**, *359*, 1139–1143. [CrossRef]
72. Chen, G.; Gang, W.Z.; Chang, X.C.; Wang, N.; Zhang, P.F.; Cao, Q.Y. Paleoproductivity of the Chang 7 unit in the Ordos Basin (North China) and its controlling factors. *Palaeogeogr. Palaeoclimatol. Palaeoecol.* **2020**, *551*, 109741. [CrossRef]
73. House, B.M.; Norris, R.D. Unlocking the barite paleoproductivity proxy: A new high–throughput method for quantifying barite in marine sediments. *Chem. Geol.* **2020**, *552*, 119664. [CrossRef]
74. Lu, S.F.; Zhang, M.; Zhong, N.N. *Oil and Gas Geochemistry*; Petroleum Industry Press: Beijing, China, 2008.
75. Dymond, J.; Suess, E.; Lyle, M. Barium in Deep–Sea Sediment: A Geochemical Proxy for Paleoproductivity. *Paleoceanography* **1992**, *7*, 163–181. [CrossRef]
76. Wang, R.Y.; Hu, Z.Q.; Nie, H.K.; Liu, Z.B.; Chen, Q.; Gao, B.; Liu, G.X.; Gong, D.J. Comparative analysis and discussion of shale reservoir characteristics in the Wufeng-Longmaxi and Niutitang formations. *Pet. Geol. Exp.* **2018**, *40*, 639–649. (In Chinese with English abstract)

77. Li, D.L.; Li, R.X.; Tan, C.Q.; Zhao, D.; Xue, T.; Zhao, B.S.; Khaled, A.; Liu, F.T.; Xu, F. Origin of silica, paleoenvironment, and organic matter enrichment in the Lower Paleozoic Niutitang and Longmaxi formations of the northwestern Upper Yangtze Plate: Significance for hydrocarbon exploration. *Mar. Pet. Geol.* **2019**, *103*, 404–421. [CrossRef]
78. Ross, D.J.K.; Bustin, R.M. Investigating the use of sedimentary geochemical proxies for paleoenvironment interpretation of thermally mature organic–rich strata: Examples from the Devonian–Mississippian shales, Western Canadian Sedimentary Basin. *Chem. Geol.* **2009**, *260*, 1–19. [CrossRef]
79. Schenau, S.J.; Reichart, G.J.; Lange, G. Phosphorus burial as a function of paleoproductivity and redox conditions in Arabian Sea sediments. *Geochim. Cosmochim. Acta* **2005**, *69*, 919–931. [CrossRef]
80. Shen, J.; Schoepfer, S.D.; Feng, Q.L.; Zhou, L.; Yu, J.X.; Song, H.Y.; Wei, H.Y.; Algeo, T.J. Marine productivity changes during the end–Permian crisis and Early Triassic recovery. *Earth Sci. Rev.* **2015**, *149*, 136–162. [CrossRef]
81. Jones, B.; Manning, D.A.C. Comparison of geochemical indices used for the interpretation of palaeoredox conditions in ancient mudstones. *Chem. Geol.* **1994**, *111*, 111–129. [CrossRef]
82. Algeo, T.J.; Tribovillard, N. Environmental analysis of paleoceanographic systems based on molybdenum–uranium covariation. *Chem. Geol.* **2009**, *268*, 211–225. [CrossRef]
83. Kurek, M.R.; Harir, M.; Shukle, J.T.; Schroth, A.W.; Schmitt-Kopplin, P.; Druschel, G.K. Seasonal transformations of dissolved organic matter and organic phosphorus in a polymictic basin: Implications for redox-driven eutrophication. *Chem. Geol.* **2021**, *573*, 120212. [CrossRef]
84. Severmann, S.; Anbar, A. Reconstructing Paleoredox Conditions through a Multitracer Approach: The Key to the Past Is the Present. *Elements* **2009**, *5*, 359–364. [CrossRef]
85. Algeo, T.J.; Li, C. Redox classification and calibration of redox thresholds in sedimentary systems. *Geochim. Cosmochim. Acta* **2020**, *287*, 8–26. [CrossRef]
86. Bau, M.; Dulski, P. Distribution of yttrium and rare-earth elements in the Penge and Kuruman iron–formations, Transvaal Supergroup, South Africa. *Precambrian Res.* **1996**, *79*, 37–55.
87. Wignall, P.B.; Twitchett, R.J. Oceanic anoxic and the end Permian mass extinction. *Science* **1996**, *272*, 1155–1158. [CrossRef]
88. Zhang, M.L.; Guo, W.; Shen, J.; Liu, K.; Zhou, L.; Feng, Q.L.; Lei, Y. New progreses on geochemical indicators of ancient oceanic redox condition. *Geol. Sci. Technol. Inf.* **2017**, *36*, 95–106, (In Chinese with English abstract).
89. Algeo, T.J.; Liu, J.S. A re-assessment of elemental proxies for paleoredox analysis. *Chem. Geol.* **2020**, *540*, 119549. [CrossRef]
90. Elderfield, H.; Greaves, M.J. The rare earth elements in seawater. *Nature* **1982**, *296*, 214–219. [CrossRef]
91. Wignall, P.B.; Newton, R.; Brookfield, M.E. Pyrite framboid evidence for oxygenpoor deposition during the Permian-Triassic crisis in Kashmir. *Palaeogeogr. Palaeoclimatol. Palaeoecol.* **2005**, *216*, 183–188. [CrossRef]
92. Zhou, C.M.; Jiang, S.Y. Palaeoceanographic redox environments for the lower Cambrian Hetang Formation in South China: Evidence from pyrite framboids, redox sensitive trace elements, and sponge biota occurrence. *Palaeogeogr. Palaeoclimatol. Palaeoecol.* **2009**, *271*, 279–286. [CrossRef]
93. Helz, G.R.; Miller, C.V.; Charnock, J.M.; Mosselmans, J.F.W.; Pattrick, R.A.D.; Garner, C.D.; Vaughan, D.J. Mechanism of molybdenum removal from the sea and its concentration in black shales: EXAFS evidence. *Geochim. Cosmochim. Acta* **1996**, *60*, 3631–3642. [CrossRef]
94. Rowe, H.D.; Loucks, R.G.; Ruppel, S.C.; Rimmer, S.M. Mississippian Barnett Formation, Fort Worth Basin, Texas: Bulk geochemical inferences and Mo–TOC constraints on the severity of hydrographic restriction. *Chem. Geol.* **2008**, *257*, 16–25. [CrossRef]
95. Tribovillard, N.; Algeo, T.J.; Baudin, F.; Riboulleau, A. Analysis of marine environmental conditions based onmolybdenum-uranium covariation-Applications to Mesozoic paleoceanography. *Chem. Geol.* **2012**, *324–325*, 46–58. [CrossRef]
96. Algeo, T.J.; Rowe, H. Paleoceanographic applications of trace-metal concentration data. *Chem. Geol.* **2012**, *324–325*, 6–18. [CrossRef]